

# Probing general relativistic spin-orbit coupling with gravitational waves from hierarchical triple systems

Marius A. Oancea,<sup>1,\*</sup> Richard Stiskalek,<sup>2,3,†</sup> and Miguel Zumalacárregui<sup>4,‡</sup>

<sup>1</sup>*University of Vienna, Faculty of Physics, Boltzmannngasse 5, 1090 Vienna, Austria*

<sup>2</sup>*Astrophysics, University of Oxford, Denys Wilkinson Building, Keble Road, Oxford, OX1 3RH, UK*

<sup>3</sup>*Universitäts-Sternwarte, Ludwig-Maximilians-Universität München, Scheinerstr. 1, 81679 München, Germany*

<sup>4</sup>*Max Planck Institute for Gravitational Physics (Albert Einstein Institute), Am Mühlenberg 1, D-14476 Potsdam, Germany*

Wave packets propagating in inhomogeneous media experience a coupling between internal and external degrees of freedom and, as a consequence, follow spin-dependent trajectories. These are known as spin Hall effects, which are well known in optics and condensed matter physics. Similarly, the gravitational spin Hall effect is expected to affect the propagation of gravitational waves on curved spacetimes. In this general-relativistic setup, the curvature of spacetime acts as impurities in a semiconductor or inhomogeneities in an optical medium, leading to a frequency- and polarization-dependent propagation of wave packets. In this letter, we study this effect for strong-field lensed gravitational waves generated in hierarchical triple black hole systems in which a stellar-mass binary merges near a more massive black hole. We calculate how the gravitational spin Hall effect modifies the gravitational waveforms and show its potential for experimental observation. If detected, these effects will bear profound implications for astrophysics and tests of general relativity.

**Introduction.** In optics and condensed matter physics, the dynamics of wave packets carrying intrinsic angular momentum can generally depend on spin-orbit interactions [1–3]. This mechanism describes the mutual coupling between the external (average position and momentum) and internal (spin or polarization) degrees of freedom of the wave packet and is generally responsible for the spin Hall effects [1, 2, 4, 5]. These effects have been observed in several experiments [6–9], and have led to a broad range of applications in spintronics, photonics, metrology, and optical communications [5, 10, 11].

Similarly, spin-orbit interactions are also predicted to affect the dynamics of wave packets in gravitational fields through the gravitational spin Hall effect (GSHE), be it for electromagnetic [12–15] or linearized gravitational [16, 17] waves propagating on curved spacetimes (see also Refs. [18–21]). This implies a certain universality of spin Hall effects across different physical systems. The analogy that we can make between the general relativistic setup and other areas of physics is that black holes (BHs) in spacetime play a role similar to impurities in a semiconductor or inhomogeneities of an optical medium. Thus, under the influence of gravity, wave packets carrying intrinsic angular momentum (as is the case with electromagnetic and gravitational waves) follow frequency- and polarization-dependent trajectories, reducing to geodesic motion only in the limit of infinite frequency, i.e. geometrical optics (GO). Given this frequency dependence, we expect gravitational waves (GWs) to represent the most favorable avenue for observing the GSHE.

GWs offer a precision probe of astrophysical phenomena [22, 23], carrying information on strong field dynamical gravity. Due to their low frequency, the GSHE is much less suppressed for GWs than for electromagnetic signals. A fraction of GW sources may merge in a high-

curvature region. For example, active galactic nuclei (AGNs) or globular cluster binary formation channels [24, 25] provide ideal candidates for a detectable GSHE signal. As the number of recorded GW events grows, so will the prospect of such a detection.

In this letter, we present compelling theoretical and numerical evidence for astrophysical configurations for which the GSHE is measurable on GW signals at the current detector sensitivity in optimal situations. We will discuss the GSHE, its imprint on waveforms, and the prospects for detection. A more detailed account of our results can be found in our companion paper, Ref. [26].

**Gravitational spin Hall effect.** We investigate the lensing of GWs in hierarchical triple BH systems, where two stellar-mass BHs merge and emit GWs in the proximity of the third, much larger BH, which acts as a lens. We assume that the merging BHs are much smaller than the lens, so that we can use the following idealized model: the lens is represented by a fixed background Kerr BH, and the merging BHs are treated as a static point source of GWs. The emitted GWs are treated as small metric perturbations of the background Kerr BH, and are described by the linearized Einstein field equations.

In the GO approximation, the propagation of GWs is described by the null geodesics of the background spacetime [27, Sec. 35.13]. However, this does not take into account the general relativistic spin-orbit coupling between the internal and external degrees of freedom of a wave packet. This appears as higher-order corrections to the GO approximation [12, 13, 16], resulting in frequency- and polarization-dependent wave packet propagation (GSHE). The equations of motion that describe

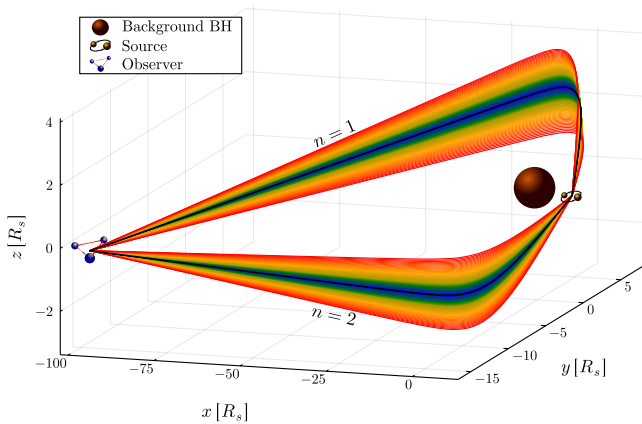


Figure 1. Two bundles of GSHE trajectories connecting a source at  $(5R_s, \pi/2, 0)$  to an opposite observer. The background BH is Kerr with  $a = 0.99M$ . For each bundle we plot the  $s = \pm 2$  trajectories deviating from the geodesic trajectory (black line) with increasing  $\epsilon$ .

the GSHE are [13, 16]

$$\dot{x}^\mu = p^\mu + \frac{1}{p \cdot t} S^{\mu\beta} p^\nu \nabla_\nu t_\beta, \quad (1a)$$

$$\dot{x}^\nu \nabla_\nu p_\mu = -\frac{1}{2} R_{\mu\nu\alpha\beta} p^\nu S^{\alpha\beta}. \quad (1b)$$

Here, external degrees of freedom are represented by  $x^\mu(\tau)$ , the worldline of the energy centroid of the wave packet, and the average wave packet momentum  $p_\mu(\tau)$ . The internal degree of freedom is represented by the spin tensor  $S^{\alpha\beta}$ , which encodes the angular momentum carried by the wave packet. The timelike vector field  $t^\alpha$  represents the 4-velocity of observers that describe the dynamics of the wave packet [13] and  $R_{\mu\nu\alpha\beta}$  is the Riemann tensor. Here, we consider circularly polarized wave packets, for which the spin tensor is uniquely fixed as

$$S^{\alpha\beta} = \frac{\epsilon s}{p \cdot t} \epsilon^{\alpha\beta\gamma\lambda} p_\gamma t_\lambda, \quad (2)$$

where  $s = \pm 2$ , depending on the state of circular polarization,  $\epsilon$  is the Levi-Civita tensor and  $\epsilon$  defined as

$$\epsilon = \frac{c^2 \lambda}{GM} \approx 0.1 \left( \frac{40 \text{ Hz}}{f} \right) \left( \frac{5 \times 10^4 M_\odot}{M} \right), \quad (3)$$

is the wavelength  $\lambda$  of the GW in units of the background black hole mass  $M$ , with  $f$  being the frequency. The GSHE vanishes if  $\epsilon \rightarrow 0$  and Eq. (1) reduce to the geodesic equations of GO.

We model the hierarchical triple BH system as a Kerr background BH of mass  $M$  and spin parameter  $a$ , together with a static source of GWs placed close to the BH and a distant static observer. We use Eq. (1) to study the propagation of GWs between the source and the observer. The GSHE will be seen by the observer

as a time delay between the frequency and polarization components of the waveform.

In Fig. 1, we show an example of two  $\epsilon s$ -parameterized bundles of trajectories that connect a source and an observer. Typically, there exist two distinct bundles of trajectories that directly connect a source and an observer, and several other bundles of trajectories that loop around the BH. We shall mainly focus on the directly connecting bundles and ignore the ones that loop around the black hole, as the latter correspond to highly demagnified signals. The connecting trajectories are determined numerically, as outlined in Ref. [26, Sec. II.C]. This also yields the time of arrival of an  $\epsilon s$ -parameterized ray intersecting with the observer's worldline.

**Time delays.** The GSHE ray propagation induces a frequency- and polarization-dependent time of arrival. The observer proper time of arrival along the  $n^{\text{th}}$  bundle is denoted by  $\tau_{\text{GSHE}}^{(n)}(f, s)$ , and we write the time delays as

$$\Delta\tau^{(n)}(\epsilon, s) = \tau_{\text{GSHE}}^{(n)}(\epsilon, s) - \tau_{\text{GO}}^{(n)}, \quad (4a)$$

$$\Delta\tau_{\text{R-L}}^{(n)}(\epsilon) = \tau_{\text{GSHE}}^{(n)}(\epsilon, s = +2) - \tau_{\text{GSHE}}^{(n)}(\epsilon, s = -2), \quad (4b)$$

where  $\tau_{\text{GO}}^{(n)}$  is the geodesic proper time of arrival. The first equation is the dispersive GSHE-to-geodesic delay, and the second is the birefringent delay between the right- and left-polarized rays. We find that both the GSHE-to-geodesic and right-to-left delays can be well approximated as a power law in frequency with proportionality factor  $\beta$  and exponent  $\alpha$  as

$$\Delta\tau \approx \beta \sqrt{-g_{00}|_{\mathbf{x}_{\text{obs}}}} \left( \frac{2c}{R_s} \frac{1}{f} \right)^{\alpha-1} \frac{1}{f}, \quad (5)$$

where  $R_s = 2GM/c^2$  is the Schwarzschild radius of the background BH. For the GSHE-to-geodesic delay we denote the power law parameters by  $\alpha, \beta$  and in the case of the birefringent delay by  $\alpha_{\text{R-L}}, \beta_{\text{R-L}}$ .

We find  $\alpha \approx 2$  and  $\alpha_{\text{R-L}} \approx 3$ , independently of the configuration. On the other hand, the proportionality factors  $\beta$  and  $\beta_{\text{R-L}}$  are determined by the mutual orientation of the source and the observer with respect to the background BH and its spin. The origin of the power law scaling and the dependence of the GSHE on the configuration are discussed in Ref. [26, Sec. III.A]. Note that  $\beta_{\text{R-L}}$  is typically subdominant, but only zero in the Schwarzschild metric.

**Gravitational waveforms.** The GSHE-induced time delay measured by the observer is frequency-dependent and weakly polarization-dependent. A gravitational waveform in a terrestrial detector typically spans a frequency range 50 – 1000 Hz and therefore its frequency components are delayed – either positively or negatively, depending on the sign of  $\beta$  – with respect to the original waveform emitted by the source. The frequency components of the unlensed waveform  $\tilde{h}_0(f, s)$  are

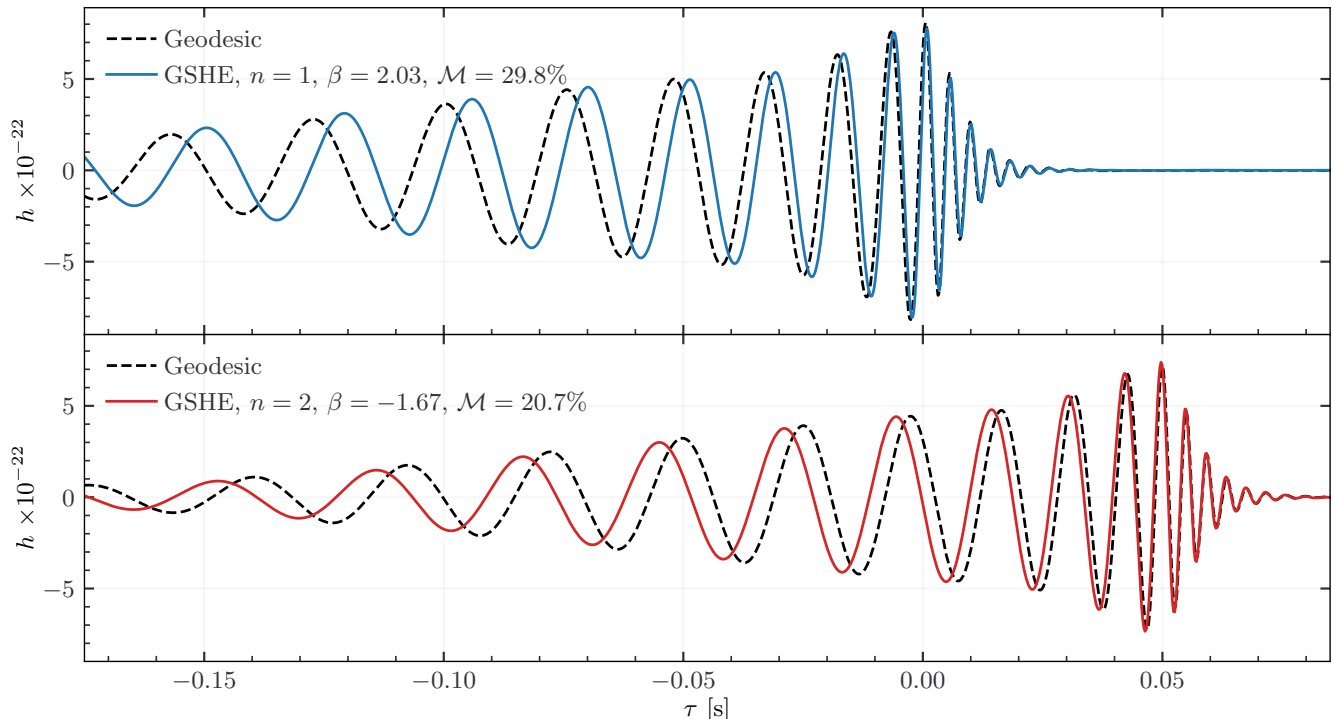


Figure 2. The waveform of a 50 and 35  $M_{\odot}$  merger propagated along the two  $n$ -indexed bundles shown in Fig. 1 (top and bottom rows). The geodesic delay between bundles is  $\tau_{\text{GO}}^{(2)} - \tau_{\text{GO}}^{(1)} = 50$  ms for this configuration. We assume  $\lambda_{\text{max}}/R_s = 0.1$ , where  $\lambda_{\text{max}}$  is the largest wavelength at 40 Hz, and report the mismatch  $\mathcal{M}$ . The GSHE is a frequency-dependent phase shift in the inspiral part of the the signal.

phase shifted so that in the circular polarization basis the GSHE-corrected waveform is

$$\tilde{h}_{\text{GSHE}}(f, s) = \sum_n e^{-2\pi i f \Delta\tau^{(n)}(f, s)} \sqrt{|\mu^{(n)}(f, s)|} \tilde{h}_0(f, s). \quad (6)$$

The sum runs over the different images, that is, the bundles connecting the source and observer [26, Sec. II.E]. The magnification factor  $\mu^{(n)}$  has a negligible dependence on  $f$  and  $s$ , so we will use the GO limit [26, Sec. II.B].

In Fig. 2, we show an example of the GSHE-induced frequency-dependent delay on an IMRPhenomXP [28] waveform of a 50 and 35  $M_{\odot}$  binary BH merger. The merger frequency is  $\sim 225$  Hz, we set the lower frequency limit to 40 Hz and the background BH mass  $M = 5 \times 10^4 M_{\odot}$ . In this case, the maximum value of  $\epsilon$  is 0.1, and the GSHE-to-geodesic delay is

$$\Delta\tau \approx 3 \text{ ms } \beta \left( \frac{5 \times 10^4 M_{\odot}}{M} \right) \left( \frac{40 \text{ Hz}}{f} \right)^2. \quad (7)$$

Due to the inverse quadratic scaling with frequency, the delay of the merger components is  $\sim 30$  times less than that of the early inspiral at 40 Hz. The GSHE introduces a frequency-dependent phase shift in the inspiral part of the waveform, which is analogous to a nonzero graviton mass if  $\beta > 0$  [26, Sec. IV.E].

As a measure of distinguishability of the GSHE imprint on the waveform, we calculate the mismatch  $\mathcal{M}$  assuming a flat detector sensitivity [26, Sec. II.E]. In Fig. 2, for the configuration given in Fig. 1, we find that for the two bundles  $\beta \approx 2$  and  $-1.7$  and thus  $\mathcal{M} \approx 30$  and 21 %. The GSHE is clearly distinguishable even for a moderate signal-to-noise ratio (SNR) [29]. We further assess detectability using the equivalence of the GSHE (in the limit  $\Delta\tau_{\text{L-R}} \sim 0$ ) to tests of the modified dispersion relation for GWs, as both predict a phase shift  $\propto 1/f^2$  on the waveform. Posterior samples of the analyzed LIGO-Virgo-Kagra (LVK) events [30–32] translate into  $\sim \mathcal{O}(10^{-2})$  90% c.l. limits on  $|\beta|$ , assuming  $M = 5 \times 10^4 M_{\odot}$  [26, Sec. II.D], in good agreement with the mismatch criterion.

**Detectability.** Throughout this work, we have assumed a fiducial background BH mass of  $5 \times 10^4 M_{\odot}$ . In this regime, the wavelength of GWs detectable by terrestrial observatories is sufficiently large to deviate from the GO propagation without requiring a wave optics treatment [33, 34] – the regime in which our GSHE calculation applies. We identify two favorable configurations that yield  $|\beta| \gtrsim 1$ : aligned source and observer (Fig. 1) and non-aligned source-observer, where a strongly deflected trajectory grazes the shadow of the background BH. Both configurations are apparent in Fig. 3, where

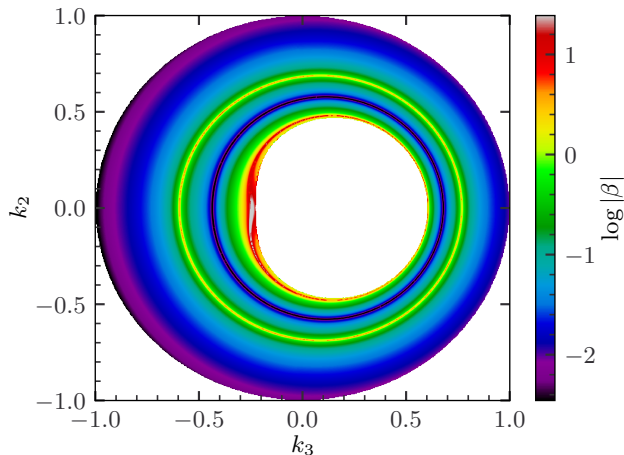


Figure 3. The GSHE-to-geodesic delay magnitude  $\beta$  as a function of the initial emission directions from the source computed with  $\epsilon_{max} = 0.01$ . These are parameterized by Cartesian coordinates  $k_2$  and  $k_3$  on the celestial sphere of the source, and the central white region represents the background BH shadow. The source is placed at  $(5 R_s, \pi/2, 0)$  and the “observer” is defined as the point where the  $\epsilon_{max}$  trajectory intersects the sphere of radius  $50 R_s$ . Each pixel represents an  $\epsilon$  bundle of trajectories.

the dispersive GSHE amplitude is shown as a function of the emission direction for a source at  $(5 R_s, \pi/2, 0)$  (following Ref. [26, Sec. III.A.3]). The outer ring of  $|\beta| \gtrsim 1$  corresponds to magnified bundles of trajectories toward observers closely aligned with the source-BH system. The inner region around the BH shadow boundary consists of bundles that are strongly deflected or even loop around the BH. These trajectories reach non-aligned observers but are strongly demagnified.

We calculate that in the scenario of Fig. 3, approximately 5% of the initial directions on the source celestial half-sphere facing the BH yield  $|\beta| \gtrsim 0.5$ , further scaling as the inverse square of the radial source distance from the background BH. Translating probabilities to the observer frame introduces a Jacobian element  $|\mu|^{-1}$ . This reflects how magnified images require a precise source-lens-observer alignment, while demagnified images are generic: there is at least one strongly deflected trajectory grazing the light ring and reaching any observer. Trajectories with  $|\mu| \ll 1$  and  $|\beta| \gtrsim 1$  are the primary contributors to the probability, even when accounting for demagnification.

To estimate the detection probabilities, we define the effective GSHE observable volume

$$V_G = \int dz \frac{dV_z}{dz}(z) \int d|\mu| P_{\text{det}} \frac{d\Upsilon_{\text{obs}}}{d|\mu|}, \quad (8)$$

via an integral over source redshift and magnification of the product of comoving differential volume  $dV_z/dz$ , detected fraction  $P_{\text{det}}$  [35] and probability of observable

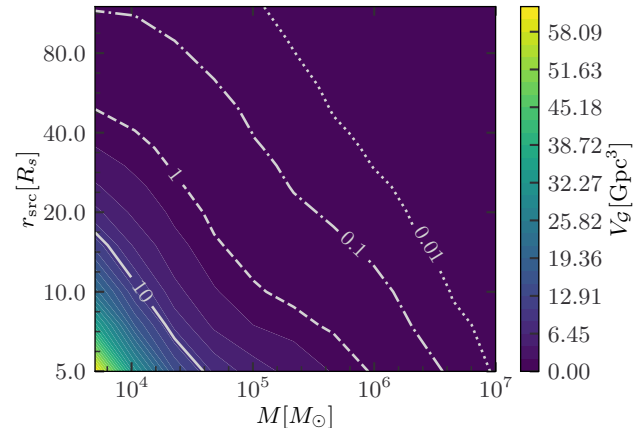


Figure 4. Effective volume for a  $30 + 30 M_\odot$  non-spinning binary observed by Cosmic Explorer, as a function of the distance to the background BH and its mass.

GSHE in the observer sphere  $d\Upsilon_{\text{obs}}/d|\mu|$ , both depending on the sources’ properties and SNR. Fig. 4 shows  $V_G$  for quasi-circular, non-spinning  $30 + 30 M_\odot$  binary coalescences observed by Cosmic Explorer [36] as a function of the mass of the background BH and its distance to the source (see Ref. [26, Sec. II.E] for details). The detection rate is  $\dot{N}_{\text{obs}} \approx \mathcal{R} V_G$ , where the merger rate  $\mathcal{R}(M, r_{\text{src}})$  is assumed to be constant.

Configurations where the GSHE is detectable may be realized in dense, dynamical environments, such as globular and nuclear star clusters [37–39]. These regions are expected to host a population of stellar- and intermediate-mass BHs: stellar binaries may then merge close to a more massive object, either by chance or because of its effect on the binary. In the most favorable case,  $r_{\text{src}} \sim 5 R_s$  and  $M \sim 5 \times 10^4 M_\odot$ , next-generation detectors reach an effective volume  $\sim 30 \text{ Gpc}^3$ . Another potential scenario consists of stellar-mass binary BHs in AGNs. There, BHs are expected to migrate radially inward due to interactions with the gas and become trapped close to the innermost stable circular orbit of the background BH [40] (red region in Fig. 4). In this case, the high mass of the background BH  $\gtrsim 10^7 M_\odot$  severely suppresses the chance of observation by ground detectors. Nevertheless, our calculation is conservative in this limit, as our simulations do not resolve well the high  $\beta$  regime, which dominates the probabilities for large  $M$ .

The GSHE is a promising probe of the BH merger environment due to the frequency-dependent time delay. In addition, we expect to receive multiple, shortly spaced, images of the same merger along various bundles connecting the source and observer. The delay between the images and their relative magnification can be used to retrieve information about the BH mass and the orientation of the source-BH-observer system. The GSHE may add additional information, including a direct constraint

on the background BH spin if the birefringence effect  $\Delta\tau_{R-L}$  is observed.

**Conclusion.** We analyzed the GSHE on lensed gravitational waveforms. The GSHE is a strong field effect that describes the propagation of polarized wave packets, such as GWs. The GSHE produces a frequency-dependent delay in the inspiral part of the waveform, while keeping the merger and ringdown relatively unchanged, as shown in Fig. 2. The delay has a characteristic dispersive  $1/f^2$  dependence, mimicking a nonzero graviton mass when  $\beta > 0$  and may appear as a violation of Einstein’s theory if not correctly taken into account.

We identified two promising scenarios for the detection of the GSHE. One in which the source and observer are aligned, leading to magnified images, and the second in which the two are not aligned but the image is strongly deflected. Both cases require the GW source to be sufficiently close to the background BH at  $\sim 10 R_s$ . AGNs and globular clusters might be favorable environments for such events. Although the number of such events is unknown [24], next-generation ground detectors are likely to detect the GSHE from sources within  $\mathcal{O}(30)R_s$  from intermediate mass BHs. The dependence on background BH mass and source frequency implies that detection prospects will be best for lighter BHs and low-frequency space-borne detectors [41–46]. This will require developing the GSHE beyond GO [47] and static sources.

A detection of the GSHE in agreement with general relativity will be a strong indication of a binary merging close to an intermediate-mass or massive BH. It would directly inform binary formation scenarios, probe their close environment, and provide exquisite constraints on a large class of alternative gravity theories [48, 49]. In summary, GW observations offer potential for experimental verification of the GSHE. The GSHE is a compelling probe of GWs propagating in strong gravitational fields, potentially enabling novel applications in astrophysics and fundamental physics.

The authors thank Lars Andersson, Pedro Cunha, Dan D’Orazio, Bence Kocsis, Johan Samsing, Laura Sberna, and Jochen Weller for input and discussions. RS acknowledges financial support from STFC Grant No. ST/X508664/1 and the Deutscher Akademischer Austauschdienst (DAAD) Study Scholarship.

---

\* [marius.oancea@univie.ac.at](mailto:marius.oancea@univie.ac.at)

† [richard.stiskalek@physics.ox.ac.uk](mailto:richard.stiskalek@physics.ox.ac.uk)

‡ [miguel.zumalacarregui@aei.mpg.de](mailto:miguel.zumalacarregui@aei.mpg.de)

- [1] K. Y. Bliokh, F. J. Rodríguez-Fortuño, F. Nori, and A. V. Zayats, Spin-orbit interactions of light, *Nature Photonics* **9**, 796 (2015).
- [2] J. Sinova, S. O. Valenzuela, J. Wunderlich, C. H. Back, and T. Jungwirth, Spin Hall effects, *Reviews of Modern Physics* **87**, 1213 (2015).
- [3] A. Manchon, H. C. Koo, J. Nitta, S. M. Frolov, and R. A. Duine, New perspectives for Rashba spin–orbit coupling, *Nature Materials* **14**, 871 (2015).
- [4] M. I. Dyakonov and A. V. Khaetskii, Spin Hall Effect, in *Spin Physics in Semiconductors*, edited by M. I. Dyakonov (Springer Berlin Heidelberg, 2008) pp. 211–243.
- [5] X. Ling, X. Zhou, K. Huang, Y. Liu, C.-W. Qiu, H. Luo, and S. Wen, Recent advances in the spin Hall effect of light, *Reports on Progress in Physics* **80**, 066401 (2017).
- [6] A. A. Bakun, B. P. Zakharchenya, A. A. Rogachev, M. N. Tkachuk, and V. G. Fleisher, Observation of a surface photocurrent caused by optical orientation of electrons in a semiconductor, *Soviet Journal of Experimental and Theoretical Physics Letters* **40**, 1293 (1984).
- [7] Y. K. Kato, R. C. Myers, A. C. Gossard, and D. D. Awschalom, Observation of the spin Hall effect in semiconductors, *Science* **306**, 1910 (2004).
- [8] O. Hosten and P. Kwiat, Observation of the spin Hall effect of light via weak measurements, *Science* **319**, 787 (2008).
- [9] K. Y. Bliokh, A. Niv, V. Kleiner, and E. Hasman, Geometrodynamics of spinning light, *Nature Photonics* **2**, 748 (2008).
- [10] T. Jungwirth, J. Wunderlich, and K. Olejník, Spin Hall effect devices, *Nature Materials* **11**, 382 (2012).
- [11] S. Liu, S. Chen, S. Wen, and H. Luo, Photonic spin Hall effect: fundamentals and emergent applications, *Opto-Electronic Science* **1**, 220007 (2022).
- [12] M. A. Oancea, J. Joudioux, I. Y. Dodin, D. E. Ruiz, C. F. Paganini, and L. Andersson, Gravitational spin Hall effect of light, *Physical Review D* **102**, 024075 (2020).
- [13] A. I. Harte and M. A. Oancea, Spin Hall effects and the localization of massless spinning particles, *Physical Review D* **105**, 104061 (2022).
- [14] V. P. Frolov, Maxwell equations in a curved space-time: Spin optics approximation, *Physical Review D* **102**, 084013 (2020).
- [15] P. Gosselin, A. Bérard, and H. Mohrbach, Spin Hall effect of photons in a static gravitational field, *Physical Review D* **75**, 084035 (2007).
- [16] L. Andersson, J. Joudioux, M. A. Oancea, and A. Raj, Propagation of polarized gravitational waves, *Physical Review D* **103**, 044053 (2021).
- [17] N. Yamamoto, Spin Hall effect of gravitational waves, *Physical Review D* **98**, 061701 (2018).
- [18] L. Andersson and M. A. Oancea, Spin Hall effects in the sky, [arXiv:2302.13634](https://arxiv.org/abs/2302.13634) (2023).
- [19] M. A. Oancea, C. F. Paganini, J. Joudioux, and L. Andersson, An overview of the gravitational spin Hall effect, [arXiv:1904.09963](https://arxiv.org/abs/1904.09963) (2019).
- [20] M. A. Oancea and A. Kumar, Semiclassical analysis of Dirac fields on curved spacetime, *Physical Review D* **107**, 044029 (2023).
- [21] Z. Li, J. Qiao, W. Zhao, and X. Er, Gravitational Faraday Rotation of gravitational waves by a Kerr black hole, *Journal of Cosmology and Astroparticle Physics* **2022** (10), 095.
- [22] The LIGO Scientific Collaboration, Advanced LIGO, *Classical and Quantum Gravity* **32**, 074001 (2015).
- [23] The LIGO Scientific Collaboration and the Virgo Collaboration, Observation of Gravitational Waves from a Binary Black Hole Merger, *Physical Review Letters* **116**,

- 061102 (2016).
- [24] D. Gerosa and M. Fishbach, Hierarchical mergers of stellar-mass black holes and their gravitational-wave signatures, *Nature Astronomy* **5**, 749 (2021).
- [25] J. Samsing, I. Bartos, D. J. D’Orazio, Z. Haiman, B. Kocsis, N. W. C. Leigh, B. Liu, M. E. Pessah, and H. Tagawa, AGN as potential factories for eccentric black hole mergers, *Nature* **603**, 237 (2022).
- [26] M. A. Oancea, R. Stiskalek, and M. Zumalacárregui, From the gates of the abyss: Frequency- and polarization-dependent lensing of gravitational waves in strong gravitational fields, [arXiv:2209.06459](https://arxiv.org/abs/2209.06459) (2022).
- [27] C. W. Misner, K. S. Thorne, and J. A. Wheeler, *Gravitation* (W. H. Freeman San Francisco, 1973).
- [28] G. Pratten, C. García-Quirós, M. Colleoni, A. Ramos-Buades, H. Estellés, M. Mateu-Lucena, R. Jaume, M. Haney, D. Keitel, J. E. Thompson, and S. Husa, Computationally efficient models for the dominant and subdominant harmonic modes of precessing binary black holes, *Physical Review D* **103**, 104056 (2021).
- [29] L. Lindblom, B. J. Owen, and D. A. Brown, Model waveform accuracy standards for gravitational wave data analysis, *Physical Review D* **78**, 124020 (2008).
- [30] B. P. Abbott *et al.* (LIGO Scientific, Virgo), Tests of General Relativity with the Binary Black Hole Signals from the LIGO-Virgo Catalog GWTC-1, *Physical Review D* **100**, 104036 (2019).
- [31] R. Abbott *et al.* (LIGO Scientific, Virgo), Tests of general relativity with binary black holes from the second LIGO-Virgo gravitational-wave transient catalog, *Physical Review D* **103**, 122002 (2021).
- [32] R. Abbott *et al.* (LIGO Scientific, VIRGO, KAGRA), Tests of General Relativity with GWTC-3, [arXiv:2112.06861](https://arxiv.org/abs/2112.06861) (2021).
- [33] G. Tambalo, M. Zumalacárregui, L. Dai, and M. H.-Y. Cheung, Lensing of gravitational waves: efficient wave-optics methods and validation with symmetric lenses, [arXiv:2210.05658](https://arxiv.org/abs/2210.05658) (2022).
- [34] C. Leung, D. Jow, P. Saha, L. Dai, M. Oguri, and L. V. E. Koopmans, Wave Mechanics, Interference, and Decoherence in Strong Gravitational Lensing, [arXiv:2304.01202](https://arxiv.org/abs/2304.01202) (2023).
- [35] H.-Y. Chen, D. E. Holz, J. Miller, M. Evans, S. Vitale, and J. Creighton, Distance measures in gravitational-wave astrophysics and cosmology, *Classical Quantum Gravity* **38**, 055010 (2021).
- [36] D. Reitze *et al.*, Cosmic Explorer: The U.S. Contribution to Gravitational-Wave Astronomy beyond LIGO, *Bulletin of the American Astronomical Society* **51**, 035 (2019).
- [37] R. M. O’Leary, B. Kocsis, and A. Loeb, Gravitational waves from scattering of stellar-mass black holes in galactic nuclei, *Monthly Notices of the Royal Astronomical Society* **395**, 2127 (2009).
- [38] M. A. S. Martinez *et al.*, Black Hole Mergers from Hierarchical Triples in Dense Star Clusters, *The Astrophysical Journal* **903**, 67 (2020).
- [39] M. A. Sedda, S. Naoz, and B. Kocsis, Quiescent and Active Galactic Nuclei as Factories of Merging Compact Objects in the Era of Gravitational Wave Astronomy, *Universe* **9**, 138 (2023).
- [40] P. Peng and X. Chen, The last migration trap of compact objects in AGN accretion disc, *Monthly Notices of the Royal Astronomical Society* **505**, 1324 (2021).
- [41] P. Amaro-Seoane *et al.*, Laser Interferometer Space Antenna, [arXiv:1702.00786](https://arxiv.org/abs/1702.00786) (2017).
- [42] J. Baker *et al.*, The Laser Interferometer Space Antenna: Unveiling the Millihertz Gravitational Wave Sky, [arXiv:1907.06482](https://arxiv.org/abs/1907.06482) (2019).
- [43] Y. Gong, J. Luo, and B. Wang, Concepts and status of Chinese space gravitational wave detection projects, *Nature Astronomy* **5**, 881 (2021).
- [44] M. A. Sedda *et al.*, The missing link in gravitational-wave astronomy: discoveries waiting in the dechertz range, *Classical and Quantum Gravity* **37**, 215011 (2020).
- [45] V. Baibhav *et al.*, Probing the nature of black holes: Deep in the mHz gravitational-wave sky, *Experimental Astronomy* **51**, 1385 (2021).
- [46] A. Sesana *et al.*, Unveiling the gravitational universe at  $\mu$ -Hz frequencies, *Experimental Astronomy* **51**, 1333 (2021).
- [47] V. Cardoso, F. Duque, and G. Khanna, Gravitational tuning forks and hierarchical triple systems, *Physical Review D* **103**, L081501 (2021).
- [48] J. M. Ezquiaga and M. Zumalacárregui, Gravitational wave lensing beyond general relativity: Birefringence, echoes, and shadows, *Physical Review D* **102**, 124048 (2020).
- [49] S. Goyal, A. Vijaykumar, J. M. Ezquiaga, and M. Zumalacárregui, Probing lens-induced gravitational-wave birefringence as a test of general relativity, [arXiv:2301.04826](https://arxiv.org/abs/2301.04826) (2023).